ACS chemical biology

ACS AuthorChoice

Articles

pubs.acs.org/acschemicalbiology

Terms of Use

Platinum-RNA Modifications Following Drug Treatment in *S. cerevisiae* Identified by Click Chemistry and Enzymatic Mapping

Maire F. Osborn, Jonathan D. White, Michael M. Haley, and Victoria J. DeRose*

Department of Chemistry and Biochemistry, University of Oregon, Eugene, Oregon 97403, United States

Supporting Information

ABSTRACT: With the importance of RNA-based regulatory pathways, the potential for targeting noncoding and coding RNAs by small molecule therapeutics is of great interest. Platinum(II) complexes including cisplatin (*cis*-diamminedichloroplatinum(II)) are widely prescribed anticancer compounds that form stable adducts on nucleic acids. In tumors, DNA damage from Pt(II) initiates apoptotic signaling, but this activity is not necessary for cytotoxicity (e.g., Yu *et al.*, 2008), suggesting accumulation and consequences of Pt(II) lesions on non-DNA targets. We previously reported an azide-functionalized compound, picazoplatin, designed for post-treatment click labeling that enables detection of Pt complexes (White *et al.*, 2013). Here, we report in-gel fluorescent detection of Pt-bound rRNA and tRNA extracted from picazoplatin-treated *S. cerevisiae* and labeled using Cu-free click chemistry. These data provide the first evidence that cellular tRNA is a platinum drug substrate. We assess Pt(II) binding sites within rRNA from cisplatin-treated *S. cerevisiae*, in regions where damage is linked to significant downstream consequences including the sarcin-ricin loop (SRL) Helix 95. Pt-RNA adducts occur on the nucleotide substrates of ribosome-inactivating proteins, as well as on the bulged-G motif critical for elongation factor recognition of the loop. At therapeutically relevant concentrations, Pt(II) also binds robustly within conserved cation-binding pockets in Domains V and VI rRNA at the peptidyl transferase center. Taken together, these results demonstrate a convenient click chemistry methodology that can be applied to identify other metal or covalent modification-based drug targets and suggest a ribotoxic mechanism for cisplatin cytotoxicity.

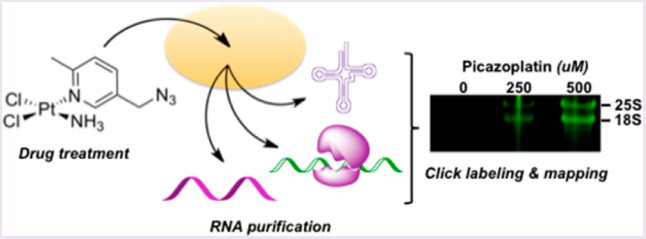

Cisplatin is the preeminent compound within the class of widely prescribed platinum(II) anticancer therapeutics. These small molecules form exchange-inert cross-links with a variety of biomolecular targets, particularly across neighboring purine bases of nucleic acids. Formation of irreparable cross-links on DNA induces programmed cell death in tumors.[1] However, as less than 10% of intracellular cisplatin accumulates on DNA, cytotoxicity and alternative cell death pathways caused by additional Pt modifications are a major interest.[2,3] We are specifically interested in assessing Pt modifications in cellular RNA, which may be a significant additional target acting as either molecular decoy or synergistic player in cisplatin-induced toxicity. For *Saccharomyces cerevisiae*, we have previously shown that cisplatin-derived Pt-RNA adducts are more prevalent than in DNA.[4] Cisplatin binding has been observed *in vitro* within rRNA,[4,5] tRNA,[6] siRNA,[7−9] and miRNA,[10] but it is not known to what extent these RNAs are targeted in cellular conditions, where accessibility may be modulated by binding partners and Pt concentrations mediated by other factors. Platinum lesions on RNA are not expected to be well-tolerated; disruptions to RNA-based processes where structure and function are tightly coupled, such as rRNA synthesis, splicing, and translation, have been observed in cell extracts or *in vitro*.[11−14] Moreover, there is developing recognition that RNA damage may contribute to cellular apoptotic signaling.[15,16] There is a clear need to characterize the molecular RNA targets of platinum, especially those that may initiate cytoplasmic cytotoxicity.

Here, we show in-gel visualization of post-treatment labeled RNA-Pt adducts acquired upon in-cell treatment with Pt compounds. We also characterize, to nucleotide resolution, Pt(II) binding within the sarcin-ricin loop and peptidyl transferase center of the ribosomal large subunit. These studies show the potential for ribotoxic response to chemotherapies, as well as structural insight into the accessibility of unique RNA structures to metal complexes *in vivo*.

RESULTS AND DISCUSSION

Click Fluorescent Tagging and Identification of Pt-Bound RNA. We recently developed a method to detect platinum-modified targets through bioorthogonal ligation of Pt-bound species to alkyne-containing fluorescent probes (Scheme 1).[17] Post-treatment modification allows the Pt compound to bind without potential interference from attached labels, such as fluorescent dyes. Despite the prevalence of Pt therapeutics, the only other example of this approach was a recent application to acridine-modified Pt compounds.[18] Here, we use picazoplatin, an azide-functionalized click-capable derivative

Received: May 19, 2014
Accepted: July 23, 2014
Published: July 23, 2014

Scheme 1. (a) Platinum(II) Therapeutics Cisplatin, Oxaliplatin, Picoplatin, and Click-Capable Picazoplatin. (b) Cu-Free Fluorescent Labeling of a Picazoplatin-Bound Nucleic Acid with Alexa Fluor 488 DIBO Alkyne

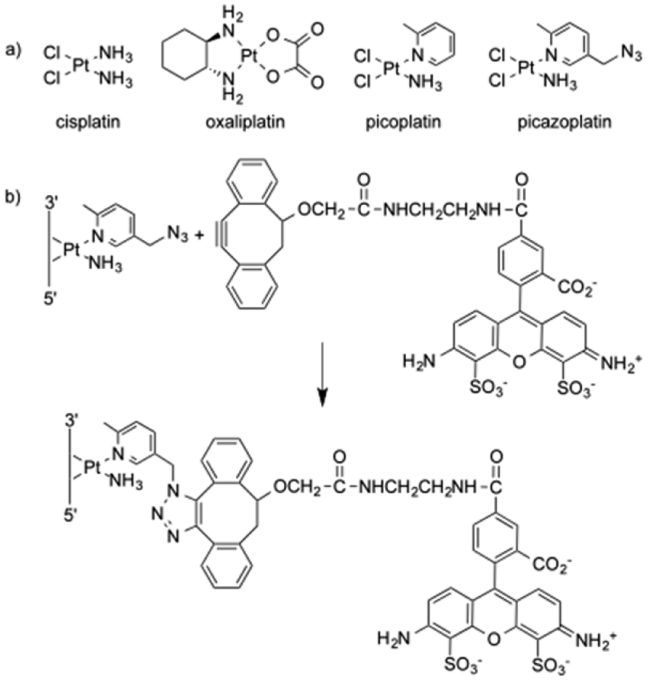

of picoplatin,[17] to observe dose-dependent fluorescent post-labeling of *S. cerevisiae* rRNA and tRNA (Figure 1). In-gel fluorescence scanning reveals significant labeling of the 25S, 18S, 5.8S, and 5S rRNA bands. The broad distribution of fluorescent labeling between all ribosomal subunits demonstrates the environmental accessibility of rRNA toward stable Pt modifications *in vivo*. This approach allows a rough quantification of Pt lesions per RNA based on signal intensity, with an estimated detection limit of ~1 Pt per 10,000 nt (see Supporting Information). Using this calculation, we estimate ~0.5 platinum molecules per ribosome following treatment with 250 μM picazoplatin (Supplementary Table S1). This value agrees well with previous ICP-MS quantification of platinum accumulation as 1−2 per ribosome following 6 h treatment with 100 or 200 μM cisplatin,[4] especially since picoplatin, the picazoplatin parent compound, has slower substitution kinetics.[19,20] Interestingly, significant fluorescence is observed in the smaller 70−100 nt tRNAs, especially at the lower (250 μM) picazoplatin concentration. On the basis of the signal intensity in this population of RNA, it appears that Pt is accumulating on the order of ~0.4 Pt per tRNA (Supplementary Table S1).

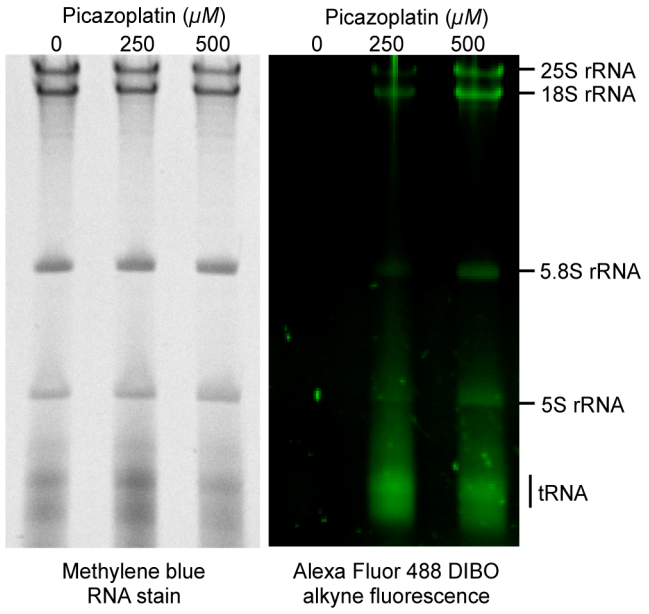

Figure 1. Fluorescent analysis of post-labeled Pt-bound rRNA and tRNA purified from picazoplatin-treated *S. cerevisiae*. Cells were treated with 0, 250, or 500 μM picazoplatin for 6 h. Harvested RNAs (~5 μg) were reacted with an excess of Alexa Fluor 488 DIBO alkyne (18 h, 37 °C), RNeasy column purified, and analyzed via 10% dPAGE. Dose-dependent labeling of tRNA and 25S, 18S, 5.8S, and 5S rRNA is observed. Fluorescence (right) colored for clarity using Adobe Photoshop. Experimental conditions provided in Methods.

To our knowledge, this is the first indication of *in vivo* Pt(II) accumulation in tRNA. The functional consequences of Pt-tRNA adducts are unknown but could be predicted to perturb their regulatory function. For instance, damage to tRNAs directly impacts RNA metabolism, may be a cellular signal of oxidative stress, and is indirectly linked to enhanced apoptotic signaling due to an increase in free cytochrome *c*.[16,21,22] The observation of the accumulation of Pt(II) species on tRNA is especially intriguing given that damaged tRNAs, once sensed, are expected to have reduced half-lives, sometimes as short as minutes.[23] However, given that tRNAs are already highly modified RNA species that fold into complex and diverse tertiary structures, their function may be more tolerant to Pt lesions. For example, certain nucleotide modifications are suggested to exert stabilizing effects by restricting conformational flexibility,[24] thus reducing the propensity for enzymatic or base-catalyzed degradation. As an additional factor, cisplatin lesions prevent exo- and endonuclease digestion of a number of RNA species.[25] An accumulation of Pt-bound tRNA could result in nuclear mislocalization, as is observed for unspliced or modified tRNAs.[26] Furthermore, elevated levels of tRNAs are implicated in some disease states.[27,28]

Enzymatic Mapping of Pt(II) Adducts in *S. cerevisiae* Ribosomal RNA. In rRNA, sites that are functionally susceptible to deleterious substitutions, metal ion-mediated cleavage, or structural modifications are clustered in domains V and VI, within the functional core of the ribosome.[29−32] Certain modifications in these domains are capable of initiating a ribotoxic stress response in actively translating ribosomes, and we hypothesize that Pt-induced modifications in these regions may contribute to cisplatin cytotoxicity.[33,34] One particularly sensitive rRNA motif is the sarcin-ricin loop (SRL), a universally conserved and purine-rich 12 nt sequence located adjacent to the peptidyl transferase center (PTC) (Figure 2). The SRL (*S. cerevisiae* helix 95) folds into an energetically stable distorted hairpin containing several non-Watson−Crick base pairs and unique motifs, including a GAGA tetraloop, a bulged G-motif, an S-turn, and a terminal A-form duplex.[35] It scaffolds critical protein−RNA interactions within the ribosome and is the target of ribosome inactivating proteins (RIPs) such as α-sarcin and ricin, proteins that catalytically modify the capping loop of the SRL, inhibiting the elongation step of translation and inducing apoptosis.[36] Point mutations and structural perturbations within the SRL, such as those that may be induced by platinum cross-linking, are lethal.[36,37] Additionally,

dx.doi.org/10.1021/cb500395z | *ACS Chem. Biol.* 2014, 9, 2404−2411

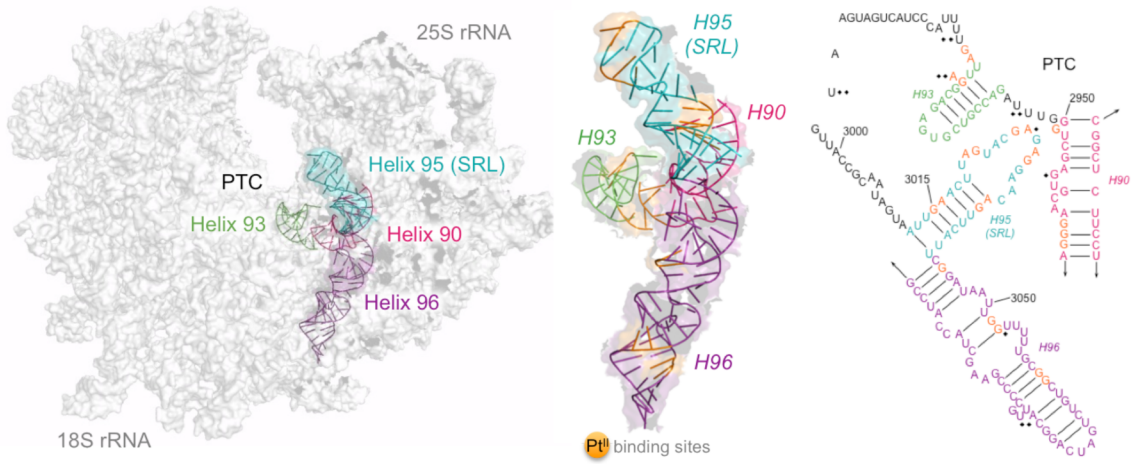

Figure 2. Model of cisplatin-derived platinum binding within helices 90, 93, 95, and 96 of the *S. cerevisiae* large ribosomal subunit RNA. Crystal structure of rRNA (PDB 3O30, 3O5H) is shown with probed regions highlighted in color and expanded to show predicted platinum dinucleotide cross-links in orange (middle). Cross-links agree well with proposed solvent accessibility and nucleotide position according to the crystal structure. Pt(II) sequence specificity is summarized on the right, with sites of moderate (◆) and high (◆◆) SHAPE reactivity overlaid.[42] The 2D structure map of yeast rRNAs was obtained from the Comparative RNA Web site.[49]

the SRL is proposed to host several cation-binding pockets, which could facilitate platinum coordination.[38] Therefore, given the structural properties of this motif and potential for its modification to cause significant downstream consequences, we have carefully examined Pt adduct accumulation in the SRL of RNA isolated from *S. cerevisiae* following cisplatin treatment.

Primer extension analysis, in which a reverse transcriptase stalls 3′ to a platinum adduct,[4,5] was used to identify platinum binding pockets in the region of the SRL (helices 95 and 96, Figure 3, Supplementary Figures S1 and S2) and adjacent solvent-accessible and mobile helices in the PTC (helices 90 and 93, Supplementary Figure S3). Such cross-links are expected to primarily occur between the N7 positions of purines that are in close proximity. Within the *S. cerevisiae* SRL, extension data using two different primers (A and B) provides clear evidence for concentration-dependent platinum adducts (Figure 3, Supplementary Figures S1 and S2). With both primers, we observe a strong stop in the SRL stem at U3037, indicative of a 5′-ApG-3′ adduct between A3035:G3036 (Figure 3, Supplementary Figure S2). In DNA helices, this sequence is known to be kinetically preferred over the opposite 5′-GpA-3′.[39] In the highly conserved and purine-rich terminal SRL loop, multiple stop sites arise in RNA isolated from cells treated with increasing cisplatin concentrations (Figure 3, Supplementary Figures S1 and S2). For comparison, we extended these studies to investigate *in vitro* platinum binding within a SRL oligomer (vide infra). In Figure 3, the multiple stop sites in the region between G3033 and G3026 indicate that platinum binding *in vivo* in or near to this loop causes structures that are nonpermissive to RT extension. While it is difficult to identify specific platinum adducts, line plot analyses for both primers suggest a primary stop site within this region at A3029 (Supplementary Figure S2) or G3028 (Figure 3), suggesting formation of a Pt(II) adduct between G3028:A3027 or a monofunctional adduct at A3027. A3027 is moderately reactive in *in vivo* SHAPE analyses, indicating some degree of conformational flexibility.[42] Ricin specifically depurinates A3027, while α-sarcin cleaves the phosphodiester backbone between A3027 and G3028, and both types of damage

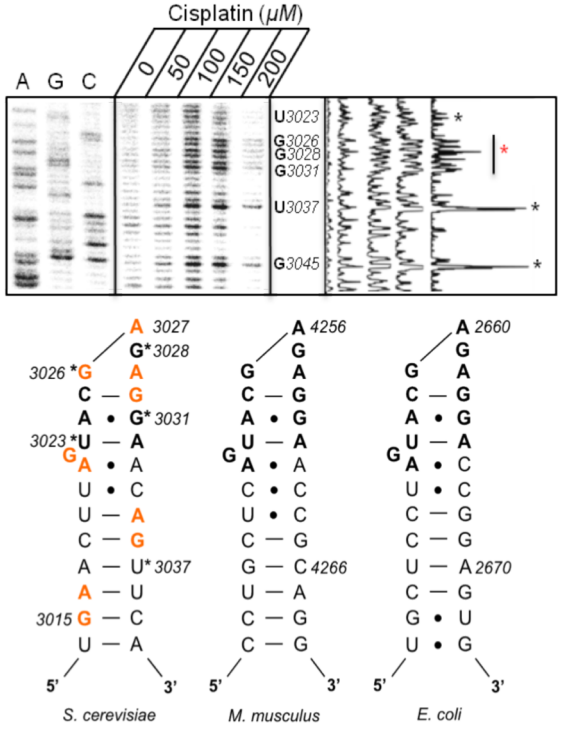

Figure 3. Primer extension analysis of the sarcin-ricin loop (SRL) region in rRNA extracted from *S. cerevisiae* treated with 0−200 μM cisplatin (using SRL primer A). Dideoxy sequencing ladder labeled by A, U, C, and G. Cisplatin-induced stop sites are denoted by asterisks (*) and represent nucleotides 3′ to a stable platinum adduct. Colored asterisk denotes primary stop site in terminal SRL region (at G3028) according to line plot analysis. Predicted platinum cross-links based on analysis are colored on the *S. cerevisiae* secondary structure map (including 5′-GA-3′ adduct between G3015:A3016 from data shown in Supplementary Figure S2). The 12 nt universally conserved RNA sequence is in bold. *M. musculus* and *E. coli* sequences are provided for comparison.

culminate in apoptosis.[34] We hypothesize that the observed Pt(II) lesions may elicit a similar ribotoxic response.

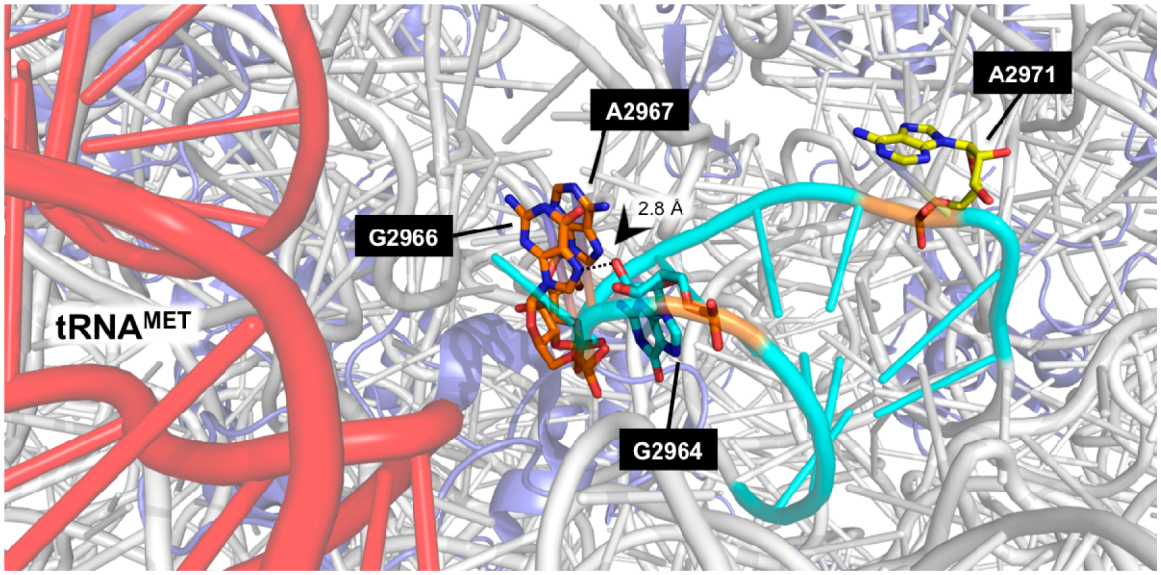

Figure 4. Model depicting H93 (aqua) in the context of a $tRNA^{Met}$-bound ribosome (tRNA: red; rRNA: gray; protein: light purple). G2966 and A2967 in the terminal loop of H93 (orange) are organized around a ~2.8 Å hydrogen bond to the 2′OH of the G2964 ribose sugar (aqua). A2971 (yellow) is clearly flipped out from the helix and in a position accessible for Pt(II). Figure generated in PyMOL using PDB files 4BYR, 4BYO, 4BYQ, and 4BYL.[50]

Toward the 5′ side of the GAGA tetraloop, a region most clearly probed using the "upstream" SRL primer B, a clear stop site occurs at U3023 (Supplementary Figure S2), indicating Pt(II) binding at the bulged-G motif (G3022) critical for loop recognition by elongation factor 2 (EF-G, *E. coli*).[40] Depending on the flexibility of this non-Watson−Crick basepaired nucleotide, this could represent a monofunctional Pt(II) adduct on G3022 or a 5′-ApG-3′ adduct between A3021:G3022. Disruption of RNA-protein interactions at G3022 is directly linked to translation inhibition and ribotoxic response signaling.[40,41] The final clear stop within the sarcin-ricin loop is at the 5′ distal end of the helix (Figure 2), where RT extension shows unusually strong Pt-induced stops at A3017 (Supplementary Figure S2). As this is a relatively purine-rich stretch of the stem, one possible cause would be a 5′-GpA-3′ Pt diadduct between G3015:A3016.

Throughout helix 96, which sequentially neighbors the SRL, platinum accumulation is observed on adjacent purines at therapeutically relevant treatment conditions as low as 100 μM cisplatin, which we have previously correlated with a cytoplasmic concentration of 47 μM.[4] In regions of duplex RNA and longer hairpins, we generally observe stable 3′-GG-5′ Pt(II) intrastrand adducts. In regions which may exhibit flexibility, such as the H95:H96:H97 three-helix junction,[43] primer extension is terminated on the first guanine of a 3′-GG-5′ pair (G3045:G3044), suggesting a monofunctional adduct or long-range RNA cross-link (Figures 2, 3, S1).

One facet of cisplatin's effect on RNA-dependent cellular processes is the inhibition of translation elongation.[44] We therefore assessed platinum binding within helix 93, one of the mobile stalks of the peptidyl transferase center (Supplementary Figure S3). This structure is adjacent to the aa-tRNA accommodation corridor and hosts A2971 in its stem. This particular adenine is the most conformationally flexible residue in the PTC and was found to be strongly reactive to SHAPE 2′−OH modification in E. *coli* and *S. cerevisiae* in the absence of tRNA in purified ribosomes.[42] Moreover, mutations at A2971 strongly interfere with peptide release.[30] From our primer mapping data, a strong stop site at G2973 suggests that A2971 is also highly reactive to platinum cross-linking, forming a cross-link with G2972 (Supplementary Figure S3). These data suggest that the Pt(II) adduct occurred in an A-site tRNA-unbound (i.e., Pt(II) accessible) state, providing a mechanism to inhibit further translation. Intriguingly, although the broad reactivity of platinum toward adjacent purines is well established, cisplatin binding in this region is remarkably specific; several purines in helix 93 (G2956, A2957, G2965, A2966, G2967, and A2968) are unreactive toward Pt(II). Figure 4 depicts H93 in the context of a $tRNA^{Met}$-bound ribosome.[50] In this structure, the purine nucleotides G2966 and A2967 in the terminal loop of H93 (orange) are organized around a ~2.8 Å hydrogen bond between the N7 of G2966 and the 2′OH of the G2964 ribose sugar (aqua). This interaction may preclude stable Pt(II) diadduct formation between G2966:A2967, and explain a general mechanism for protection at this loop. However, A2971 (yellow) is clearly flipped out from the helix and in an accessible position. This may account for our observation of strong targeting to A2971, while the H93 terminal loop appears shielded (Supplementary Figure S3).

In this investigation of Pt(II) adduct formation within the PTC, we also uncovered several Pt(II) binding sites in helix 90, corresponding to 1,2-intrastrand GpG adducts (Figure 2). These results are somewhat obscured by the prevalence of RNA modifications within these sequences (Supplementary Figure S3). However, they clearly depict the ability of Pt(II) to target accessible purine bases within a complex RNA structure. The summary of these analyses is presented in the rRNA secondary structure map in Figure 2.

Enzymatic Mapping of Pt(II) Adducts in a Model SRL RNA. To compare SRL RNA accessibility to Pt *in vivo* with an *in vitro* model, platinum adducts within a 27 nt model SRL oligomer were probed using primer extension analysis. From NMR structural data and molecular simulations, this sequence is known to fold into a stable structure *in vitro*, allowing our 27 nt oligomer to accurately model the SRL in the context of the 25S rRNA.[35,45] We have assessed aquated ("activated")

dx.doi.org/10.1021/cb500395z | *ACS Chem. Biol.* 2014, 9, 2404−2411

cisplatin binding within the SRL from 0—2 equiv (Figure 5). We observe dose-dependent platinum stop sites occurring at

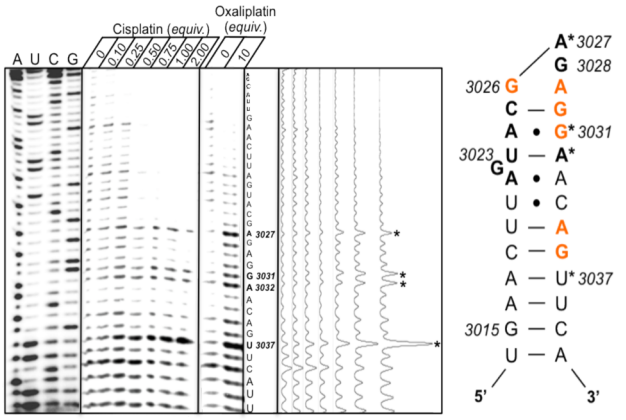

Figure 5. Primer extension analysis of a folded model *S. cerevisiae* sarcin-ricin loop RNA following treatment (20 h, 37 °C) with 0—2 equiv of aquated cisplatin or 0—10 equiv of nonaquated oxaliplatin (using SRL primer A). Cisplatin-induced dose-dependent stop sites are denoted by asterisks. Oxaliplatin-induced stop sites mimic those of cisplatin and are shown for comparison. Mapping results are summarized in the secondary structure diagram using the same notation as in Figure 3.

U3036, A3031, G3030, and A3026 (*S. cerevisiae* numbering). The platinum adducts predicted by these stop sites are highlighted in color in the *S. cerevisiae* secondary structure map. They include a canonical 3′-GG-5′ adduct (G3031:G3030), two putative 3′-GA-5′ intrastrand cross-links (G3036:A3035; G3030:A3029), and a signal at an isolated guanine that could represent a monofunctional adduct or a cross-link bridging the terminal GAGA tetraloop (G3026). As described earlier, there is a strong causal link between damage at this position and downstream apoptotic signaling. It is important to note that under these conditions each RNA may be bound by multiple Pt(II) atoms. Due to the 3′ bias of this technique, it is difficult to define where 1,2-intrastrand Pt(II) lesions form on the 5′ distal region of the duplex.

Cisplatin accumulation within the model SRL was compared to the RT stalling pattern following SRL treatment with nonactivated oxaliplatin (Figure 5). The equilibria, mechanism, and rates of aquation and binding differ between cisplatin and oxaliplatin and depend strongly on pH and ionic environment.[46] For oxaliplatin, dissociation of the oxalato ligand is reported to occur with a half-life of 92 min at 37 °C.[47] In our 18-h incubation, 10 equiv of nonactivated oxaliplatin are required to observe RNA-Pt(II) adducts, compared with just 0.5—1 equiv of activated cisplatin. Remarkably, despite these differences, their kinetically preferred binding sites are identical within the SRL. Conservation of Pt(II) binding within the SRL may demonstrate a ubiquitous mechanism for translation inhibition.

Finally, we report that the pattern of platinum accumulation within the GAGA tetraloop differs slightly between the sarcin-ricin loop *in vitro* model and the *in vivo* and presumably intact ribosome (Figure 6). For RNA isolated following *in vivo* treatment, we observe Pt(II) accumulation within A3027 and G3028 by two different primer extension assays. However, neither nucleotide is Pt(II)-bound in our *in vitro* model (Figure 6). This may be explained in part by *anti*/*syn* base flipping of

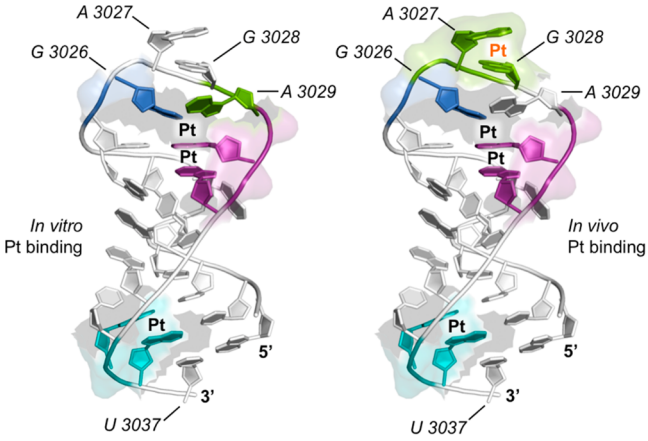

Figure 6. Model comparing differences in Pt(II) binding preferences within the SRL *in vitro* and *in vivo*. Predicted platinum adducts are denoted by "Pt". Pt(II) binding is conserved throughout the SRL with the exception of the GAGA tetraloop. *In vivo*, strong Pt(II) targeting to A3027 and G3028 (Pt, orange) is observed. This targeting is not conserved *in vitro*. Figure generated in PyMOL using PDB files 3O5H and 3O50.

the terminal adenine as predicted by molecular simulations and suggested by solution NMR studies.[35,48] According to these studies, although the SRL is highly rigid when compared to other RNA motifs, the tetraloop is dynamic. Given that several protein interactions occur *in vivo* at the tetraloop that may induce unfolding or stabilization, we predict a concurrent change in platinum accessibility and binding. The change in the binding pattern could also reflect *in vivo* RNA-protein cross-links, which are absent in our *in vitro* model.

CONCLUSION

To date, we lack a comprehensive understanding of the biological cytoplasmic substrates of Pt(II) therapeutics such as cisplatin.[3] We recently developed a method to detect platinum-modified drug targets using picazoplatin, an azide-containing picoplatin mimetic designed for post-treatment labeling via click chemistry.[17] Here, we demonstrate that rRNA and tRNA purified from picazoplatin-treated yeast accumulate platinum and are efficiently labeled with Alexa Fluor 488 DIBO alkyne to levels detectable by in-gel fluorescence (~0.5 Pt per ribosome and ~0.4 Pt per tRNA following 250 μM treatment). This is the first indication of *in vivo* accessibility of tRNA to platinum compounds. Pt-tRNA damage could severely impact cellular processes such as translation and apoptotic signaling. Within rRNA, we have explored the sarcin-ricin loop and peptidyl transferase center as high impact cisplatin targets. Using primer extension analysis, we have mapped platinum accumulation on the sarcin-ricin loop *in vivo* on rRNA extracted from yeast treated with cisplatin as well as in a model SRL oligomer. This investigation of Pt(II) adducts within Domains V and VI rRNA demonstrate a variety of potential ribotoxic roles for platinum, all of which likely contribute to the general cytotoxicity of the drug. Using picazoplatin, future avenues of research could focus on isolation, enrichment, and sequencing of platinum-bound nucleic acids to gain a global perspective on Pt accumulation and RNA access *in vivo*. We are very interested in dissecting the accumulation of cisplatin on its cellular targets with temporal resolution, as the types of Pt-RNA interactions we have described could be of cytoplasmic or nucleolar origin. Of significant interest is the potential for this azide modification

dx.doi.org/10.1021/cb500395z | *ACS Chem. Biol.* 2014, 9, 2404—2411

technique to assess the binding preferences of other small molecules on cellular RNAs.

METHODS

Platinum Drug Treatment and RNA Extraction from *S. cerevisiae*. *S. cerevisiae* strain BY4741 (MATa; his3Δ1; leu2Δ0; met15Δ0; ura3Δ0) was a generous gift from the Stevens Laboratory at the University of Oregon. Cisplatin and oxaliplatin were purchased from Sigma-Aldrich. Picazoplatin was synthesized as described previously.[17] Plated cells were grown on YEPD agar plates (1% yeast extract, 2% peptone, 2% glucose, and 2% agar). Liquid cultures were grown on Synthetic Complete medium (SC) consisting of 0.67% yeast nitrogen base and 2% glucose supplemented with amino acids and nucleotide bases and maintained in the dark at 30 °C with shaking at 200 rpm. Culture growth was measured by absorbance at 600 nm (1 AU600 = 2.0×10^7 cells/mL). A 5 mM cisplatin, oxaliplatin, or picazoplatin stock was used for all platinum treatments. Yeast cultures were pregrown to an OD_{600} of 5 (10.0×10^7 cells/mL) and then diluted to an OD_{600} of 0.25 (5.0×10^6 cells/mL) in platinum-containing media (final concentration varying between 0 and 500 μM drug). Then 10−50 mL cultures were grown for 12 h at 30 °C with shaking at 200 rpm. Total RNA was extracted from cisplatin-, oxaliplatin-, or picazoplatin-treated yeast using the MasterPure Yeast RNA Purification Kit (Epicentre) according to a modified manufacturer's protocol. Total RNA concentration was calculated using absorbance at 260 nm (1 AU = 40 μg/mL), and all samples were dried to completion by SpeedVac and resuspended in ddH_2O to a final normalized concentration of 10 ug/μL.

Fluorescent Post-Labeling of RNA from Picazoplatin-Treated *S. cerevisiae*. A 0.5 μL sample of total RNA was added to a 10 μL aqueous solution containing 0.5 μL (20 U) RiboGuard RNase Inhibitor (0.5 μL, 20 U, Epicenter) and excess Alexa Fluor 488 DIBO Alkyne (1 μL, 0.5 mM). The reaction proceeded overnight at 37 °C. Unreacted fluorophore was removed using an RNeasy mini kit (Qiagen) according to a modified manufacturer's protocol. The 20 μL eluent from the spin column was diluted with 20 μL of formamide, and the samples were analyzed on a 10% (29:1) mono/bis polyacrylamide gel. RNA purity and content were assessed with a methylene blue stain. Fluorescence images were collected with an Alpha-Imager and processed (false colored) using Adobe Photoshop.

Platination of SRL RNA *in Vitro*. Synthetic RNA was purchased from Dharmacon, consisting of the model SRL plus a short extended sequence designed for RT primer annealing (italicized). For all *in vitro* studies, cisplatin was aquated as described previously.[17] A solution of 100 μM SRL RNA (5′-UGA ACU UAG UAC GAG AGG AAC AGU UCA *CCC CCC GCC GCG AAG CUA CCA UCC GCU*-3′, typically 10 nmol) was folded by rapid heating to 90 °C and slow cooling to 4 °C in 10 mM Na_2PO_4 (pH 7.0), 100 mM $NaNO_3$, and 1 mM $Mg(NO_3)_2$. Activated cisplatin was added in 0−2-fold excess, and the mixture was incubated 37 °C for 18 h. Nonactivated oxaliplatin was added in 0−10-fold excess and incubated in identical conditions. Pt-bound RNA was purified with Sephadex G-25 Medium size exclusion resin (GE Healthcare) on laboratory prepared spin columns (BioRad) to remove unbound Pt. The eluent was dried to completion by SpeedVac, and the remaining pellet was stored at −30 °C until use.

Primer Extension Analysis of Pt-Bound RNA. DNA primers designed for reverse transcription of the model SRL and *S. cerevisiae* rRNA were purchased from Integrated DNA Technologies (5′-AGC GGA TGG TAG CTT CGC GGC-3′ for SRL primer A (also used for the *in vitro* studies), 5′-GCG TGA TCA GAC AGC CGC AAA AA-3′ for upstream SRL primer B, and 5′-CTA TTG CGG TAA CAT TCA TC-3′ for the PTC). γ-^{32}P 5′ end-labeling was performed as described previously.[25] For primer extension of a synthetically platinated RNA, 100 pmol of the prepared RNA template was annealed to 10 pmol of the SRL DNA primer with trace γ-^{32}P primer and incubated with AMV Reverse Transcriptase (Fermentas) according to a modified manufacturer's protocol for 1.75 h at 42 °C. The resulting cDNA products were diluted in loading buffer containing 0.005% (w/v) xylene cyanol and bromophenol blue and analyzed by 12% dPAGE. Bands were visualized using a GE phosphor screen in conjunction with a Storm phosphor screen imaging system. Band intensities were quantified using ImageQuant 5.1. Each band was normalized to the sum of pixel intensities in each individual lane using Microsoft Excel.

Sequencing reference lanes were generated with a Sequenase Version 2.0 DNA Sequencing kit (USB Corporation) following the manufacturer's protocol, using an appropriate DNA template (Integrated DNA Technologies) and the γ-^{32}P 5′ end-labeled primers used for the primer extension reactions.

Primer Extension Analysis of Pt-Bound RNA extracted from *S. cerevisiae*. RNA template (1 μg) was annealed to 100 pmol of the specified 5′ end-labeled primer in the manufacturer's reaction buffer and incubated in the presence of AMV Reverse Transcriptase (Fermantas) for 1.75 h at 42 °C. The resulting cDNA products were diluted in loading buffer containing 0.005% (w/v) xylene cyanol and bromophenol blue and analyzed by 8% dPAGE. Bands were visualized using a GE phosphor screen in conjunction with a Storm phosphor screen imaging system and then quantified with ImageQuant 5.1 and normalized in Excel. Sequence reference lanes were generated as described above.

Figure Preparations. All figures containing crystal structure data were prepared in PyMOL (www.pymol.org) using PDB files obtained from the RCSB Protein Data Bank.

ASSOCIATED CONTENT

Supporting Information

This material is available free of charge via the Internet at http://pubs.acs.org.

AUTHOR INFORMATION

Corresponding Author

*E-mail: derose@uoregon.edu.

Notes

The authors declare no competing financial interest.

ACKNOWLEDGMENTS

The *S. cerevisiae* strain BY4741 was a kind gift from the Stevens Laboratory. We thank Dr. R. Spitale from Stanford University for advice on *in vivo* RNA click chemistry protocols. Funding from the NIH (5T32GM007759 to M.F.O.), NSF (CHE-1153147 to V.J.D.), and the University of Oregon is gratefully acknowledged.

REFERENCES

(1) Jamieson, E. R., and Lippard, S. J. (1999) Structure, recognition, and processing of cisplatin-DNA adducts. *Chem. Rev. 99*, 2467−2498.

(2) Wisnovsky, S. P., Wilson, J. J., Radford, R. J., Pereira, M. P., Chan, M. R., Laposa, R. R., and Lippard, S. J. (2013) Targeting mitochondrial DNA with a platinum-based anticancer agent. *Chem. Biol. 20*, 1−6.

(3) Yu, F., Megyesi, J., and Price, P. M. (2008) Cytoplasmic initiation of cisplatin cytotoxicity. *Am. J. Physiol. Renal Physiol. 295*, 44−52.

(4) Hostetter, A. A., Osborn, M. F., and DeRose, V. J. (2012) RNA-Pt adducts following cisplatin treatment of *Saccharomyces cerevisiae*. *ACS Chem. Biol. 7*, 218−225.

(5) Rijal, K., and Chow, C. S. (2009) A new role for cisplatin: probing ribosomal RNA structure. *Chem. Commun. 1*, 107−109.

(6) Papsai, P., Aldag, J., Persson, T., and Elmroth, S. K. C. (2006) Kinetic preference for interaction of cisplatin with the G-C-rich wobble basepair region in both tRNAAla and MhAla. *Dalton Trans. 29*, 3515−3517.

(7) Hägerlöf, M., Papsai, P., Hedman, H. K., Jungwirth, U., Jenei, V., and Elmroth, S. K. C. (2008) Cisplatin and siRNA interference with structure and function of Wnt-5a mRNA. *J. Biol. Inorg. Chem. 13*, 385−399.

(8) Hägerlöf, M., Hedman, H., and Elmroth, S. K. C. (2007) Platination of the siRNA sense-strand modulates both efficacy and selectivity in vitro. *Biochem. Biophys. Res. Commun. 361*, 14−19.

(9) Hedman, H. K., Kirpekar, F., and Elmroth, S. K. C. (2011) Platinum interference with siRNA non-seed regions fine-tunes silencing capacity. *J. Am. Chem. Soc. 133*, 11977−11984.
(10) Polonyi, C., and Elmroth, S. K. C. (2013) Time dependence of cisplatin-induced duplex dissociation of 15-mer RNAs and mature miR-146a. *Dalton Trans. 42*, 14959−14962.
(11) Schmittgen, T. D., Ju, J. F., Danenberg, K. D., and Danenberg, P. V. (2003) Inhibition of pre-mRNA splicing by cisplatin and platinum analogs. *Int. J. Oncol. 23*, 785−789.
(12) Danenberg, P. V., Shea, L. C., Danenberg, K. D., and Horikoshi, T. (1991) Inactivation of Tetrahymena rRNA self-splicing by cis-platin proceeds through dissociable complexes. *Nucleic Acids Res. 19*, 3123−3128.
(13) Jordan, P., and Carmo-Fonseca, M. (1998) Cisplatin inhibits synthesis of ribosomal RNA in vivo. *Nucleic Acids Res. 26*, 2831−2836.
(14) Becker, J. P., Weiss, J., and Theile, D. (2013) Cisplatin, oxaliplatin, and carboplatin unequally inhibit in vitro mRNA translation. *Toxicol. Lett.*, 1−5.
(15) Bellacosa, A., and Moss, E. G. (2003) RNA repair: Damage control. *Curr. Biol. 13*, R482−484.
(16) Mei, Y., Stonestrom, A., Hou, Y.-M., and Yang, X. (2010) Apoptotic regulation and transfer RNA. *Protein Cell 1*, 795−801.
(17) White, J. D., Osborn, M. F., Moghaddam, A. D., Guzman, L. E., Haley, M. M., and DeRose, V. J. (2013) Picazoplatin, an azide-containing platinum(II) derivative for target analysis by click chemistry. *J. Am. Chem. Soc. 135*, 11680−11683.
(18) Ding, S., Qiao, X., Suryadi, J., Marrs, G. S., Kucera, G. L., and Bierbach, U. (2013) Using fluorescent post-labeling to probe the subcellular localization of DNA-targeted platinum anticancer agents. *Angew. Chem., Int. Ed. 52*, 3350−3354.
(19) Kelland, L. (2007) The resurgence of platinum-based cancer chemotherapy. *Nat. Rev. Cancer 7*, 573−584.
(20) Raynaud, F. I., Boxall, F. E., Goddard, P. M., Raynaud, I., and Goddard, M. (1997) cis-Amminedichloro(2-methylpyridine) platinum (II) (AMD473), a novel sterically hindered platinum complex: in vivo activity, toxicology, and pharmacokinetics in mice. *Clin. Cancer Res. 11*, 2063−2074.
(21) Nawrot, B., Sochacka, E., and Düchler, M. (2011) tRNA structural and functional changes induced by oxidative stress. *Cell. Mol. Life Sci. 68*, 4023−4032.
(22) Thompson, D. M., Lu, C., Green, P. J., and Parker, R. (2008) tRNA cleavage is a conserved response to oxidative stress in eukaryotes. *RNA 14*, 2095−2103.
(23) Alexandrov, A., Chernyakov, I., Gu, W., Hiley, S. L., Hughes, T. R., Grayhack, E. J., and Phizicky, E. M. (2006) Rapid tRNA decay can result from lack of nonessential modifications. *Mol. Cell 21*, 87−96.
(24) Motorin, Y., and Helm, M. (2010) tRNA stabilization by modified nucleotides. *Biochemistry 49*, 4934−4944.
(25) Chapman, E. G., and DeRose, V. J. (2010) Enzymatic processing of platinated RNAs. *J. Am. Chem. Soc. 132*, 1946−1952.
(26) Shaheen, H. H., and Hopper, A. K. (2005) Retrograde movement of tRNAs from the cytoplasm to the nucleus in Saccharomyces cerevisiae. *Proc. Natl. Acad. Sci. U.S.A. 102*, 11290−11295.
(27) Pavon-Eternod, M., Gomes, S., Geslain, R., Dai, Q., Rosner, M. R., and Pan, T. (2009) tRNA over-expression in breast cancer and functional consequences. *Nucleic Acids Res. 37*, 7268−7280.
(28) Zhou, Y., Goodenbour, J. M., Godley, L. A., Wickrema, A., and Pan, T. (2009) High levels of tRNA abundance and alteration of tRNA charging by bortezomib in multiple myeloma. *Biochem. Biophys. Res. Commun. 385*, 160−164.
(29) Dorner, S., Polacek, N., Schulmeister, U., Panuschka, C., and Barta, A. (2002) Molecular aspects of the ribosomal peptidyl transferase. *Biochem. Soc. Trans. 30*, 1131−1136.
(30) Polacek, N., and Mankin, A. S. (2005) The ribosomal peptidyl transferase center: structure, function, evolution, inhibition. *Crit. Rev. Biochem. Mol. Biol. 40*, 285−311.
(31) Winter, D., Polacek, N., Halama, I., Streicher, B., and Barta, A. (1997) Lead-catalysed specific cleavage of ribosomal RNAs. *Nucleic Acids Res. 25*, 1817−1824.
(32) Polacek, N., and Barta, A. (1998) Metal ion probing of rRNAs: evidence for evolutionarily conserved divalent cation binding pockets. *RNA 4*, 1282−1294.
(33) Iordanov, M. S., Pribnow, D., Magun, J. L., Dinh, T.-H., Pearson, J. A., and Magun, B. E. (1998) Ultraviolet radiation triggers the ribotoxic stress response in mammalian cells. *J. Biol. Chem. 273*, 15794−15803.
(34) Magun, B. E., Iordanov, M. S., Pribnow, D., Magun, J. L., and Dinh, T. (1997) Ribotoxic stress response: activation of the stress-activated protein kinase JNK1 by inhibitors of the peptidyl transferase reaction and by sequence-specific RNA damage to the alpha-sarcin/ricin loop in the 28S rRNA. *Mol. Cell. Biol. 17*, 3373−3381.
(35) Spacková, N., and Sponer, J. (2006) Molecular dynamics simulations of sarcin-ricin rRNA motif. *Nucleic Acids Res. 34*, 697−708.
(36) Shi, X., Khade, P. K., Sanbonmatsu, K. Y., and Joseph, S. (2012) Functional role of the sarcin-ricin loop of the 23S rRNA in the elongation cycle of protein synthesis. *J. Mol. Biol. 419*, 125−138.
(37) Macbeth, M. R., and Wool, I. G. (1999) Characterization of in vitro and in vivo mutations in non-conserved nucleotides in the ribosomal RNA recognition domain for the ribotoxins ricin and sarcin and the translation elongation factors. *J. Mol. Biol. 285*, 567−580.
(38) Hermann, T., and Westhof, E. (1998) Exploration of metal ion binding sites in RNA folds by Brownian-dynamics simulations. *Structure 6*, 1303−1314.
(39) Mantri, Y., Lippard, S. J., and Baik, M.-H. (2007) Bifunctional binding of cisplatin to DNA: why does cisplatin form 1,2-intrastrand cross-links with AG but not with GA? *J. Am. Chem. Soc. 129*, 5023−5030.
(40) Macbeth, M. R., and Wool, I. G. (1999) The phenotype of mutations of G2655 in the sarcin/ricin domain of 23 S ribosomal RNA. *J. Mol. Biol. 285*, 965−975.
(41) Correll, C. C., Munishkin, A., Chan, Y.-L., Ren, Z., Wool, I. G., and Steitz, T. A. (1998) Crystal structure of the ribosomal RNA domain essential for binding elogation factors. *Proc. Natl. Acad. Sci. U.S.A. 95*, 13436−13441.
(42) Leshin, J. A., Heselpoth, R., Belew, A. T., and Dinman, J. (2011) High throughput structural analysis of yeast ribosomes using hSHAPE. *RNA Biol. 8*, 478−487.
(43) Besseová, I., Réblová, K., Leontis, N. B., and Sponer, J. (2010) Molecular dynamics simulations suggest that RNA three-way junctions can act as flexible RNA structural elements in the ribosome. *Nucleic Acids Res. 38*, 6247−6264.
(44) Rosenberg, J., and Sato, P. H. (1992) Cisplatin inhibits in vitro translation of complete initiation complex by preventing the formation. *Mol. Pharmacol. 43*, 491−497.
(45) Havrila, M., Réblová, K., Zirbel, C. L., Leontis, N. B., and Sponer, J. (2013) Isosteric and nonisosteric base pairs in RNA motifs: Molecular dynamics and bioinformatics study of the sarcin-ricin internal loop. *J. Phys. Chem. B 117*, 14302−14319.
(46) Ahmad, S., Isab, A. A., and Ali, S. (2006) Structural and mechanistic aspects of platinum anticancer agents. *Transition Met. Chem. 31*, 1003−1016.
(47) Jerremalm, E., Eksborg, S., and Ehrsson, H. (2003) Hydrolysis of oxaliplatin-evaluation of the acid dissociation constant for the oxalato monodentate complex. *J. Pharm. Sci. 92*, 436−438.
(48) Warren, J. J., and Moore, P. B. (2001) Application of dipolar coupling data to the refinement of the solution structure of the Sarcin-Ricin loop RNA. *J. Biomol. NMR 20*, 311−323.
(49) Cannone, J. J., Subramanian, S., Schnare, M. N., Collett, J. R., D'Souza, L. M., Du, Y., Feng, B., Lin, N., Madabusi, L. V., Muller, K. M., Pande, N., Shang, Z., and Gutell, R. R. (2002) The comparative RNA web (CRW) site: an online database of comparative sequence and structure information for ribosomal, intron, and other RNAs. *BMC Bioinformatics 3*, 2.

(50) Fernández, I. S., Bai, X. C., Hussain, T., Kelley, A. C., Lorsch, J. R., Ramakrishnan, V., and Scheres, S. H. (2013) Molecular architecture of a eukaryotic translational initiation complex. *Science 342*, 1240585.
(51) Warner, J. R. (1999) The economics of ribosome biosynthesis in yeast. *Trends Biochem. Sci. 24*, 437−440.